Selenocysteine Positional Variants Reveal Contributions to Copper Binding from Cysteine Residues in Domains 2 and 3 of Human Copper Chaperone for Superoxide Dismutase

5 AUTHORS, INCLUDING:

Amanda Barry
Los Alamos National Laboratory
18 PUBLICATIONS   272 CITATIONS

SEE PROFILE

Adenike Otoikhian
Washington State University, Vancouver, Uni…
12 PUBLICATIONS   114 CITATIONS

SEE PROFILE

Selenocysteine Positional Variants Reveal Contributions to Copper Binding from Cysteine Residues in Domains 2 and 3 of Human Copper Chaperone for Superoxide Dismutase[†]

Amanda N. Barry[‡], **Kevin M. Clark**[§], **Adenike Otoikhian**[‡], **Wilfred A. van der Donk**[§], and **Ninian J. Blackburn**[‡]

Department of Science and Engineering, School of Medicine, Oregon Health and Sciences University, Beaverton, Oregon 97006, and Departments of Biochemistry and Chemistry, University of Illinois at Urbana-Champaign, Urbana Illinois 61801

Abstract

The human copper chaperone for superoxide dismutase binds copper both in an Atx1-like MTCQSC motif in domain 1, and via a multinuclear cluster formed by two CXC motifs at the D3 dimer interface. The composition of the Cu(I) cluster has been investigated previously by mutagenesis of the CXC motif, and by construction of a CXU selenocysteine derivative which has permitted XAS studies at both Cu and Se absorption edges. Here we report the semisynthesis and spectroscopic characterization of a series of derivatives with the sequences 243-CACA, 243-CAUA, 243-UACA and 243-UAUA in the D1 double mutant (C22AC25A) background, prepared by expressed protein ligation of Sec-containing tetrapeptides to an hCCS-243 truncation. By varying the position of the Se atom in the CXC motif, we have been able to show that Se is always bridging (2 Se-Cu) rather than terminal (1 Se-Cu). Substitution of both D3 Cys residues by Sec in the UAUA variant does not eliminate the Cu-S contribution, confirming our previous description of the cluster as most likely a Cu_4S_6 species, and suggesting that D2 Cys residues contribute to the cluster. As predicted by this model, when Cys residues C141, C144 and C227 are mutated to alanine either individually or together as a triple mutant, the cluster nuclearity is dramatically attenuated. These data suggest that Cys residues in D2 of hCCS are involved in the formation, stability and redox potential of the D3 cluster. The significance of these finding to the SOD1 thiol/disulfide oxidase activity are discussed in terms of a model in which a similar multinuclear cluster may form in the CCS-SOD heterodimer.

The copper chaperone for Cu, Zn-superoxide dismutase $(CCS)^{[1]}$, is a 27 kDa three-domain protein which carries out final post-translational processing of Cu, Zn-superoxide dismutase

---

To whom correspondence should be addressed. N.J.B Phone: (503)748−1384. Fax: (503)748−1464. Email: ninian@comcast.net.
[‡]Oregon Health and Sciences University
[§]University of Illinois

Supporting Information available. Two figures showing the Cu EXAFS of the D2 C141A/C144A/C227A triple mutant before reduction with dithionite (Figure S1) and the Cu and Se EXAFS of the cysless 243-UAUA variant before and after treatment with dithionite (Figure S2). This material is available free of charge via the Internet at http://pubs.acs.org.

[1]Abbreviations: CCS, copper chaperone for superoxide dismutase; D1, domain 1; D2, domain 2; D3, domain 3; dH_2O, deionized water; DW, Debye-Waller factor; EPL, expressed protein ligation; EXAFS, extended x-ray absorption fine structure; EZnSOD, superoxide dismutase with the copper site empty and the Zn site full; FT, Fourier transform; hCCS, human CCS; ICPOES, inductively coupled plasma optical emission spectrometry, MESNA, 2-mercapto-ethanesulfonate; Sec, selenocysteine; SOD, superoxide dismutase; TCEP, tris(2-carboxyethyl)phosphine; WT, wild type; XAS, x-ray absorption spectroscopy; yCCS, yeast CCS.

(SOD1) (1-5). The structural and functional properties of the individual domains of both the yeast (yCCS) and human (hCCS) proteins have been determined from biochemical (6,7) and crystallographic (8-11) studies. CCS-domain 1 (D1, residues 1−85) is an Atx1-like domain containing a MXCXXC Cu(I)-binding motif, but unlike other chaperones exhibiting this fold (12-16), it does not transfer copper directly to SOD1. Instead, copper transfer appears to proceed from CCS-domain 3 (D3, residues 235−274) a short unstructured polypeptide containing a CXC Cu(I)-binding motif which is absolutely required for the activity of the protein (6,7,17,18). Domain 2 (D2, residues 86−234) has remarkable sequence and structural homology to SOD, including a highly conserved dimerization interface, and in the case of the human chaperone, the retention of all of the Zn-binding and three of the four Cu-binding residues found in SOD. hCCS D2 binds one mole equivalent of Zn, but due to substitution of a His residue by Asp, is does not bind Cu in the WT protein.

The reaction chemistry of yCCS with its partner SOD has been shown to proceed via the intermediacy of a heterodimeric protein-protein interaction which was first observed in solution and subsequently characterized by crystallography. When yCCS was allowed to interact with either WT ySOD1 or a mutant (H46F) designed to be unable to bind copper (19,20), a 42kDa band was detected by gel-filtration and SDS PAGE which stained with antibodies to both proteins. The formation of the heterocomplex was sensitive to the presence of both Cu and Zn in the reaction mixture, and clearly involved the cysteine residues (C57, C146) of the SOD disulfide since it could be trapped in a C146S SOD mutant. A crystal structure of the yCCS-H46FSOD heterodimer (9) revealed that indeed, the ability to trap the intermediate was due to the formation of an intermolecular disulfide between copper ligand C229 of yCCS and C57 of SOD, and suggested a possible role for CCS in forming the SOD disulfide bond. The role of CCS in forming the essential SOD disulfide was firmly established in later studies (21,22) which demonstrated that EZnSOD^{S-H} (where E represents an empty Cu binding site) but not EZnSOD^{S-S} was the substrate for CCS, reacting with the chaperone in a Cu- and O_2-dependent manner to generate fully active CuZnSOD^{S-S}. It was proposed that the process was driven at least in part by differences in the relative stability of SOD monomers and dimers: immature EZnSOD^{S-H} was more stable in the monomeric form facilitating docking with the chaperone, whereas CuZnSOD^{S-S} was more stable as the dimer facilitating product release. More recent NMR data has suggested that while significant structural differences exist between the bis-thiol and disulfide forms, the former is not significantly destabilized, and exists as a dimer (23).

A major unresolved question is how copper catalyzes the thiol oxidase/disulfide isomerase activity of CCS. Early studies on copper binding in the presence of imidazole-, DTT and glutathione-containing buffers reported copper to protein ratios between 1 and 1.5 for both yeast (7,20,24) and human (25). In contrast, reconstitution studies in our laboratory using [Cu(MeCN)$_4$]PF$_6$ in the presence of 10% MeCN followed by exhaustive dialysis to remove excess copper and MeCN has consistently led to higher copper to protein ratios in the range $2 − 2.5$ (17,18,26). Crystallography did not determine the mode of copper binding since the structures were of apo-forms, and spectroscopic (XAS) data is only available for the human chaperone reconstituted by our [Cu(MeCN)$_4$]PF$_6$/MeCN protocol. However, our XAS data revealed that Cu(I) forms a monomeric 3-coordinate CuS$_2$X (X= exogenous thiol, or solvent) complex at the MTCQSC site in D1 but forms a cluster at the interface of two D3 polypeptides within a hCCS dimer or tetramer (17,18)}.

In recent work we have characterized a hCCS derivative containing selenocysteine (Sec, U) substituted for C246 in the D3 C^{244}XC^{246} metal-binding motif (CCS 245-Sec) (27) where combination of Cu and Se EXAFS was used to provide a more detailed description of the cluster. Studies on the CCS 245-Sec derivative of a mutant protein lacking the cysteine residues of D1 led to a description of the cluster as a Cu$_x$Se$_2$S$_y$ multinuclear species with x=3−4, and

y=2−4 (Figure 1). Each Se of the two CXU motifs in a D3 mediated dimer was bound by two Cu(I) atoms in the cluster, indicating that Cys/Sec residue 246 occupies a bridging position. Further, the high Cu-S content remaining in the Sec derivative suggested that cysteine residues other than the single remaining C244 in D3 might contribute to Cu(I) coordination in the cluster. hCCS D2 contains three cysteine residues in D2, C141, C144 and C227, and two of these C141 and C229 form an analogous disulfide to that of the SOD1 target.

One way to address this question, and further interrogate the cluster composition is to create positional Sec variants by expressed protein ligation (EPL) of Sec-containing peptides with a CCS-243 truncation. Here we report the semisynthesis and spectroscopic characterization of a series of derivatives with the sequences 243-CACA, -CAUA, -UACA and -UAUA in the D1 double mutant (C22AC25A) protein background. By varying the position of the Se atom in the CXC motif, we have been able to show that Se is always bridging (2 Se-Cu) rather than terminal (1 Se-Cu). Further, substitution of both D3 Cys residues by Sec in the D1 mutant does not eliminate the Cu-S contribution, suggesting that D2 Cys residues do indeed contribute to the cluster. When Cys residues C141, C144 and C227 are mutated to alanine either individually or together as a triple mutant, the cluster nuclearity is dramatically attenuated. These data suggest that Cys residues in D2 of hCCS are involved in the formation, stability and redox potential of the D3 cluster. The significance of these finding to the SOD1 thiol/disulfide oxidase activity are discussed in terms of a model in which a similar multinuclear cluster may form in the CCS-SOD heterodimer.

Materials and Methods

Synthesis of the tetrapeptides CACA, CAUA, UACA, and UAUA

Fmoc protected amino acids were purchased from either Advanced Chemtech (Louisville, KY) or Novabiochem (La Jolla, CA). Fmoc-Se-*p*-methoxybenzyl (PMB) selenocysteine was prepared as previously reported (28). Wang resin preloaded with Fmoc-alanine was purchased from Advanced Chemtech. Mass spectra were taken using a Waters Ultima API Quadrople Time-of-Flight (TOF) mass spectrometer at the University of Illinois-Urbana/Champaign Mass Spectrometry Laboratory.

Preparation of H$_2$N-CACA-OH

The peptide was manually synthesized on a 0.5 mmol scale using Fmoc-based chemistry. Fmoc-Ala-Wang resin was swollen in DMF (3×6 mL, 8 min). N-terminal Fmoc protection for all amino acids was removed using 20% piperidine in DMF (v/v, 3×3 min, 6 mL). A 4.5 fold excess of amino acids (2.25 mmol) was coupled to the resin-bound growing peptide in the presence of 2 equiv. of 1-hydroxybenzotriazole (HOBT) and N,N'-diisopropylcarbodiimide (DIC) (4.5 mmol) in DMF for 3 h or until qualitative Kaiser testing indicated that coupling was complete. The resin was washed extensively with CH$_2$Cl$_2$ and stored under vacuum overnight prior to cleavage. The peptide was cleaved from the resin in a cocktail of 2% triisopropylsilane/dH$_2$O/ethanedithiol in neat TFA (v/v) at RT for 2 h. The TFA was removed under reduced pressure to afford a clear oil and the peptide was precipitated as a white solid by the addition of ice-cold diethyl ether. The peptide was isolated by centrifugation at 4000 rpm for 5 min, dissolved in 1:1 CH$_3$CN/H$_2$O, and lyophilized. The crude lyophilized product was purified by preparative reverse phase HPLC on a Waters (Milford, MA) Delta Pak C18 column (130 mm $\times$ 25 mm) with a water-acetonitrile solvent system using a gradient of 2−75% solvent B over 35 min (A: H$_2$O, 0.1% TFA; B: CH$_3$CN 80% in H$_2$O v/v, 0.086% TFA). The peptide was lyophilized after purification to obtain the final product as a white solid and analyzed using TOF-electrospray ionization mass spectrometry (TOF-ESI-MS). (**CACA**: *Calculated,* 366.46; *Observed,* 367.1 (M+1)). The yield was 78.5 mg.

Preparation of H$_2$N-CAUA -OH, H$_2$N- UACA -OH, and H$_2$N-UAUA-OH

The tetramer peptides containing selenocysteine residues were manually synthesized on a 0.3 mmol scale using Fmoc-based chemistry using the protocol described above. Couplings using Fmoc-Sec(PMB)-OH were performed using a 3 fold excess of amino acid (0.84 mmol) to conserve material. The peptides were cleaved following a modified procedure of Harris et al. (29) Briefly, the peptides were cleaved in a cocktail of 2% triisopropylsilane/dH$_2$O and 2.5% thioanisole in neat TFA (v/v) containing either 7.3 equivalents of 2,2'-dithiodipyridine (pys$_2$, 2.2 mmol) for CAUA and UACA or 1.3 equivalents 2,2'-dithiobis(5-nitropyridine) (0.4 mmol) for UAUA at 25 °C for 2 h. The TFA was removed under reduced pressure to afford yellow oils from which the peptides were precipitated as yellow solids by the addition of ice-cold diethyl ether. The peptides were isolated as described above. The crude lyophilized products were purified by preparative reverse phase HPLC as described above using a gradient of 2 −100% solvent B over 45 min (A: H$_2$O, 0.1% TFA; B: CH$_3$CN 80% in H$_2$O v/v, 0.1% TFA). The peptides were lyophilized after purification to obtain the final products as white solids and analyzed by TOF-ESI-MS; (CAUA: *Calculated,* 522.5 (SH, Se(pys)); *Observed,* 522.5). (UACA: *Calculated,* 413.5 (SeH, SH), 522.5 (Se(pys), SH); *Observed,* 413.5, 522.5). (UAUA: *Calculated,* 460.25 (SeH, SeH); *Observed,* 460.1). The typical yield of the 0.3 mmol peptide scale syntheses was approximately 40 mg.

Semisynthesis of Sec-substituted hCCS derivatives

The wild type and D1 (C22AC25A) hCCS double mutants (aa 1−258) cloned in the pTXB3 intein vector (New England Biolabs) with a chitin affinity tag were constructed as previously described (18). The CCS 243- and C22AC25A 243 truncation mutants, where the Ile243 was mutated to an Ala for more efficient ligation, were created by PCR amplification of both constructs using primers at the 5' and 3' terminus 5'-ACCATGGCTTCGGATTCGGG-3' and 5'-CCGTGATGGCTCTTCCGCAGATCTGCTTGGGGTT-3'. The 243 truncations were then expressed in *E. coli* ER2566 and purified on a chitin column followed by intein cleavage by mercaptoethanesulfonic acid (MESNA). The tetrapeptides CACA, CAUA, UACA, and UAUA were ligated to the 243 truncations by methods described previously (27). Peptides were first reduced with TCEP and then added 1:10 (protein:peptide) to the truncated proteins. After 4 days of anaerobic incubation, free peptides and TCEP were removed by dialysis. Successful ligation was confirmed by ICPOES analysis of zinc and selenium concentrations and by mass spectrometry analysis. As with the previous single Sec ligation products, to circumvent the tendency towards oxidation, it was necessary to reduce the diselenide formed in the peptides with TCEP followed by rapid addition of the Cu(I) under anaerobic conditions. Proteins (in 50 mM sodium phosphate buffer, pH 7.2) were added to TCEP immobilized on agarose in a small column and left to reduce for one hour. After elution with two volumes of buffer, three mole-equivalents of [Cu(I)(CH$_3$CN]$_4^+$ in acetonitrile were immediately added to the proteins. Reconstituted proteins were then dialyzed against decreasing amounts of acetonitrile in 50 mM phosphate buffer in order to remove free copper and acetonitrile.

Protein and Metal Analysis

Protein concentration was measured by Bradford assay. Copper was measured by inductively coupled plasma optical emission spectrometry (ICPOES) on a Perkin-Elmer Optima 2000 DV spectrometer. The oxidation state of the copper was determined by electron paramagnetic resonance spectroscopy (EPR) versus a Cu(II)-ethylenediaminetetraacetic acid (EDTA) standard on a Bruker Elexys 500 EPR spectrometer. The zinc concentration was measured by ICPOES spectrometry.

Mass Spectral Analysis

Protein masses were determined by electrospray ionization mass spectrometry. Proteins were injected onto a 0.3 H 10 mm C4 column (214MS53.10;Vydac), and masses were determined on-line using an ion trap (model LCQ Deca XP plus by Thermo Finnigan). The flowrate was 9 μL/min with a linear gradient of 2−75% MeCN over 55 min in a mobile phase containing 0.1% formic acid. Samples were injected using the Surveyor autosampler (Thermo Finnigan) and concentrated/purified using a protein micro trap cartridge (Michrom BioResources). Mass spectra of proteins eluted from the C-4 column were deconvoluted using BioWorks Browser (Thermo Finnigan). Mass accuracy of better than 0.02% was confirmed using horse myoglobin.

XAS Data Collection and Analysis

Cu K-edge (8.980 keV) and Se K-edge (12.658 keV) extended x-ray absorption fine structure (EXAFS) data for the Sec positional mutants were collected at the Stanford Synchrotron Radiation Laboratory operating at 3 GeV with currents between 100 and 75 mA. All samples were measured on beam lines 7.3 or 9.3 in each case using a Si[220] monochromator and a Rh-coated mirror upstream of the monochromator with a 13 keV (Cu) or 15 keV (Se) energy cutoff to reject harmonics. On beam line 9.3, a second Rh mirror downstream of the monochromator was used to focus the beam, whereas on beam line 7.3 data were collected in unfocused mode. Data were collected as fluorescence excitation spectra using a high-count-rate Canberra 30-element Ge array detector with maximum count rates below 120 kHz. A Z-1 metal oxide (Ni, As) filter and Soller slit assembly were placed in front of the detector to reduce the elastic scatter peak. Four to six scans of a sample containing only sample buffer (50 mM $NaPO_4$, pH 7.2) were collected at each absorption edge, averaged, and subtracted from the averaged data for the protein samples to remove Z-1 K_β fluorescence and produce a flat pre-edge baseline. The samples (80 μL) were measured as aqueous glasses (>20% ethylene glycol) at 10−15 K. Energy calibration was achieved by reference to the first inflection point of a copper metal foil (8980.3 eV) for Cu K-edges and an elemental selenium foil (12658.0 eV) for Se K-edges, placed between the second and third ionization chamber. Data reduction and background subtraction were performed with the program modules of EXAFSPAK (30). Data from each detector channel were inspected for glitches, drop-outs, and other effects of non-linear fluorescence excitation before inclusion in the final average. Spectral simulation was carried out with the program EXCURVE 9.2 (31-34) as previously described (16,17,26,35).

Results and Discussion

Four tetrapeptides, CACA, CAUA, UACA and UAUA were ligated to either hCCS 243-truncation (hereafter termed WT) or its C22AC25A-243- variant (hereafter termed the D1 double mutant) to generate four separate protein variants for WT and D1 mutant respectively. These proteins contained either cysteine, selenocysteine or both at positions 244 and 246 of hCCS. The proteins were analyzed first by mass spectrometry to determine the efficiency of the ligation, and to confirm that the expected product was formed in each case. The results are shown in Table 1, and representative mass spectra for the WT and D1 UAUA ligations are shown in Figure 2. All derivatives show a dominant peak close to the mass expected for protein with the N-terminal Met residue cleaved but all spectra give less than this calculated mass by between 2 and 10 mass units with the average difference of 6 a u. This suggests the presence of ~3 disulfide or diselenide cross links. In the WT protein, a total of 3 S–S cross links are anticipated (C22-C25, C141-C227, C244-C246), whereas in the D1 C22AC25A mutant the number of cross links would be decreased by 1. The data are therefore consistent with the C/U-A-C/U motif forming either an intramolecular selenysulfide or a diselenide as was found previously for single Sec-ligated hCCS (27). Additional minor peaks (<5%) at 25517 and 25454 a.u. probably represent the unligated WT and D1 proteins respectively with the N-terminal Met residue cleaved.

Transfer activity of the Se positional variants

All of the tetrapeptide ligation constructs were assayed for activity by measuring their ability to activate EZn-SOD at a ration of 1:1 hCCS:SOD over a 30 minute incubation period. The results are listed in Table 1. With the exception of 243-CACA, variants with an intact D1 CXXC Cu(I) binding site, all show wild-type activity within experimental error, while elimination of the D1 copper binding site reduces activity by approximately twenty five per cent. Significantly, Sec substitution appears to have no deleterious effect on Cu transfer activity, regardless of its position in the D3 CXC motif, or of double substitution.

EXAFS of 243-UACA and 243-CAUA proteins

A number of structural models have been proposed for the multinuclear cluster as shown in Figure 1. Selenocysteine substitution offers a unique way of distinguishing between various models proposed for the hCCS multinuclear cluster by varying the position of the Se center within the cluster and predicting how the EXAFS is expected to change in the Se-positional isomers. In this work we have created variants 243-UACA and 243-CAUA where the position of the Se label has been interchanged, as well as the UAUA protein which carries a double Se atom substitution. The 243-CAUA variant is similar to the 245-U (243-CAU) system described previously (27). Since both Se atoms in the 245-Sec (243-CAU) D3 dimer were found to be in bridging positions coordinated to 2 Cu atoms, those in the 243-UACA D3 dimer would remain as bridging in the polynuclear cluster structures B and C, but would change to terminal positions with only a single Se-Cu bond in the simpler dinuclear cluster A (Figure 1). For the 243-UAUA variant, since both S of the CXC motif are replaced by Se, observation of Cu-S together with Cu-Se scattering in the Cu EXAFS would imply the presence of the higher order mixed S/Se polynuclear cluster C, whereas absence of Cu-S interactions are expected in the simpler all-Se clusters A and B. A particular advantage of this approach is that previously published work has already established the values of the Cu-Cu (18) and Se-Cu (27) Debye-Waller factors and these are likely to be transferable provided that the Sec-positional variants have similar static and dynamic disorder. The former is a function of the spread in the absorber-scatterer distances within a particular shell, while the latter relates to vibrational disorder, and is a function of temperature. Since (*vide infra*) the Se substitution does not appear to induce significant structural perturbation, and all XAS measurements are conducted at low temperatures (10−15 K), the conditions for transferability should be met. This has allowed us to fix the Se-Cu and Cu-Cu DW factors during refinement and thus determine coordination numbers in the Sec positional variants with more precision.

Figure 3(a) compares experimental and simulated EXAFS data at the Cu K edge for the D1 double mutant hCCS-243-UACA and CAUA proteins. The spectra overlay almost exactly and suggest that there is little difference between the Cu environments in these two proteins. Figure 3(b) compares hCCS-243-UACA and the UAUA Sec variants in the D1 double mutant background. Although still very similar, the correspondence is not as good particularly with respect to the phase of the waves at low k. Figures 4 and 5 show the results of fitting the Cu and Se EXAFS data for the UACA and UAUA proteins respectively, and the parameters used in these fits are given in Table 2. The curve fitting reproduces well both the EXAFS oscillations and the Fourier transform amplitudes.

The CACA protein (as expected) can be simulated with similar parameters to those reported previously for the C22AC25A variant of hCCS (18), although the occupation number of the Cu-Cu shell is closer to 2 rather than 3. Likewise the CAUA and UACA proteins are similar to one another, and are each close to that reported previously for the C22AC25A hCCS-243-CAC protein. Thus neither extending the C-terminus by one amino acid, nor swapping the position of the Sec residue in the CXC motif produce significant change in copper environment. The Se EXAFS of CAUA and UACA are also identical and each can be simulated by Se bonded

to two Cu atoms. Therefore, each Se atom in the cluster occupies a bridging position that is unchanged by positional substitution, and hence must be structurally equivalent. This rules out cluster geometries involving both terminal and bridging Se atoms.

EXAFS of the 243-UAUA protein

In the UAUA protein, both cysteines of the D3 CXC motif are substituted by Sec. Thus if the cluster is constituted only from UXU, the Cu EXAFS should show only Cu-Se scattering. The data in Table 2 show that this is not the case. With Cu-Se and Cu-Cu DW factors ($2\sigma^2$) fixed at 0.007 and 0.012 $Å^2$ respectively, the UAUA Cu EXAFS data are best fit by 2 Se at 2.40 Å and 1 S at 2.18 Å within a cluster of nuclearity >3 (N_{Cu-Cu} =2.6, F= 0.381). This implies that S-donors other than the D3 CXC must contribute to the cluster. Attempts to fit the data with no contribution from Cu-S gave poor results (Figure 6 and Table 2, 243-UAUA no sulfur fit, F=1.454), with an F value 3.8 times greater. The Se EXAFS data again shows 2 Se-Cu interactions, as expected for bridging Se, but are inconsistent with the simpler Cu_2Se_4 structure (Fig1 A) formed from dimerization of the CXC motif, where the combination of terminal and bridging Se would predict a Se-Cu shell occupancy of 1.5.

Mutation of D2 Cys residues to Ala

Where then could the multinuclear cluster recruit additional Cys residues? In the present work all Cys residues in the D1 CXXC and D3 CXC have been mutated or Se substituted. hCCS D2 contains an additional four Cys residues C113, C141, C144 and C227 but none of these Cys residues is conserved in the yeast protein. C141 and C227 form a disulfide cross link which is homologous to the essential C57-C146 cross link in SOD1. C144 is located close to the disulfide such that all three Cys residues C141, C144 and C227 are clustered together whereas C113 is located on the opposite side of D2, well separated from any of the metal binding sites (11). Although the location of the D3 CXC motif is disordered in the yeast homodimeric structure, and no complete structure is available for hCCS, the yCCS-SOD heterodimeric structure shows a cross link between one of the D3 Cys residues and SOD C57, thereby locating the CXC Cu binding locus potentially within coordinating distance of the D2 C141, C144, C227 cluster of Cys residues.

To explore whether these could participate in the multinuclear Cu cluster, we generated the single C141A, C144A and C227A variants and the triple C141A/C144A/C227A variant in the C22A/C25A (D1 double) background, and subjected this to Cu binding and EXAFS analysis. The results, depicted in Figure 7 and Table 3, show a significant effect of the D2 Cys residues 141, 144, and 227 on the structure and nuclearity of the cluster. When compared with the intensity of the WT D1 double mutant protein reported previously, all of the single mutants showed reduced outer shell intensity consistent with a single Cu-Cu interaction. The Cu(I) centers remained 3-coordinate as evidenced by the low intensity of the 1s→4p edge transition at 8983 eV, and the shell occupancy and bond length of the Cu-S interaction. This suggests that when any of the Cys residues in D2 are mutated, a lower-order cluster is formed with a composition consistent with a Cu_2S_4 thiolate bridged dimer (Fig. 1 A). The triple mutant behaved differently, and was isolated with more than 2 Cu but no bound Zn. Cu(I) reconstitution led initially to a species with no outer shell feature, simulating to 2 Cu-S at 2.26 Å and 1 Cu-N/O at 1.96 Å. The poor quality of the fit and high DW factors suggested a mixture of reduced and oxidized species (Figure S1), similar to those observed previously for WT hCCS expressed in the absence of Zn (26), or D3 Cys to Ala single mutants (17). As before, dithionite reduction led to a new species which could be well simulated by 3 Cu-S and 1 Cu-Cu interactions characteristic of the Cu_2S_4 thiolate-bridged dimer. It is likely that mutation of all three Cys residues in the D2 disulfide locus leads to perturbation of the Zn binding site such that it can

now bind copper, and leads to a protein species with Cu bound at both the CXC and Zn sites. As demonstrated previously (26), Cu bound at the D2 Zn site is susceptible to oxidation, but upon dithionite reduction is redistributed into the CXC Cu(I) binding site. Alternatively, the triple D2 cys mutant may lower the redox potential of the D3 CXC motif, inducing an equilibrium population of disulfide cross-linked species in D3 which cannot bind Cu. Thus, mutation of any or all of the D2 Cys residues C141, C144 or C227 converts the polynuclear Cu_4S_6 cluster to a lower order cluster consistent with the Cu_2S_4 species of Fig. 1A.

If the Cys residues of D2 are involved in formation of the polynuclear cluster, the prediction is that full Sec substitution of the D3 CXC motif in a "cysless" background should form a modified cluster with no S component in the EXAFS. We explored this prediction as follows. A variant containing the D1 double C22A/C25A and the D2 triple C141A/C144A/C227A mutations was constructed in a CCS 243 truncation construct, and this was subsequently ligated with the UAUA tetrapeptide. (We call this cysless-UAUA, although it actually contains one Cys residue C113, whose location is far from any of the metal binding sites). After TCEP reduction, this cysless-UAUA protein bound copper in a histidine-only environment (Fig. S2) suggesting that copper was bound at either the Zn center or in the vestigial Cu center of the SOD-like D2 domain. Confirmation that no copper bound at the UAUA site in D3 was obtained from Se EXAFS which showed Se-C and Se-Se interactions only (Fig. S2). This implies that the cysless variant has a modified redox potential which prevents or kinetically inhibits reduction of the diselenide at the UAUA center. The formation of either intra or inter domain diselenide bonds would explain the lack of Cu binding at the D3 site. Reduction by dithionite led to translocation of Cu(I) into a D3 cluster. Best fits to the Se data showed 1 Se-C at 1.99 Å and 2 Cu-Se interactions at 2.39 Å, while the Cu EXAFS was best fit by 2 Cu-Se at 2.37 Å and 2 −3 Cu-Cu at 2.71 Å. A small non-stoichiometric S contribution was still present in the data perhaps originating from traces of residual low molecular weight thiols (MESNA)). Therefore, the structure of the cluster in the cysless-UAUA is inconsistent with a Cu_2S_4 bis thiolate bridged entity and appears different from that observed in the D1-double, D2-triple 245-Sec in that Se remains fully bridging with multiple Cu atoms in the cluster. In this respect, the cysless-UAUA cluster more closely resembles structure B in Fig. 1. Notwithstanding, these experiments appear to support a pivotal role for D2 Cys residues C141, C144 and C227 in the cluster formation and redox potential of the D3 copper binding site.

The seemingly aberrant chemistry exhibited by the cysless UAUA protein may be symptomatic of the fact that Cu-S and Cu-Se chemistry differ in a number of respects particularly in redox potential and pK_a of the thiol or selenol. The most common multinuclear Cu(I)-thiolate clusters are based on the Cu_4S_6 adamantane type structure (Fig 1C) which is composed of three Cu_3S_3 hexagonal rings fused together (36). The Cu(I) centers are 3 coordinate and have three neighboring Cu(I) centers, with each Cu(I) ion bridged to its neighbor by a thiolate S. The Cu-Cu separation is ~ 2.7 Å. Multinuclear Cu(I) clusters can be assembled in other ways, but of those reported in the Cambridge database, few have nuclearities less than three. As discussed by Pickering and coworkers (37), more complex clusters such as Cu_5S_7 or Cu_5S_6 also contain longer Cu-Cu distances at ~2.9 − 3.0 Å, which have been identified in the EXAFS of the transcriptional activators Ace1 and Mac1 (38), but do not appear to be present in the CCS cluster. The chemistry of Cu(I) selenolate systems is not nearly as extensive, but both terminal (39) and bridging (40-42) Cu(I)-selenolate interactions are well documented with bond lengths in the range 2.30−2.45 Å, consistent with the 2.38 ± 0.02 Å Cu-Se interaction found in this and previous work (27) on Sec-substituted hCCS. In many cases, the simpler Cu_4S_X adamantane-type clusters which are common in Cu(I)-sulfur chemistry give way to multi-atom cages of Se and Cu interlocking to form complex oligomeric and polymeric structures (43, 44). However, a notable exception is the structure of a ferrocenyldiselelolate-stabilized Cu_2Se_2 cluster exhibiting a bis-selenolate bridged di-Cu(I) core in which each Cu(I) is 3-coordinate with two bridging selenolates and one terminal phosphine ligand (40). The Cu-Se

and Cu-Cu bond lengths (2.40 and 2.62 Å respectively) are close to the metrical parameters observed for the hCCS cluster. Based on these comparisons, we conclude that while differences between Cu-S and Cu-Se chemistry exist, isostructural replacement of Se for S in the cluster is not unprecedented.

Relevance to function

We have shown that hCCS in all likelihood forms two distinct clusters of different nuclearity – a polynuclear Cu_4S_6 cluster utilizing extra Cys residues from D2, and a dinuclear Cu_2S_4 cluster when these are unavailable. Yeast CCS lacks these D2 Cys residues which introduces an interesting question regarding the functional significance of the polynuclear cluster in the human chaperone. Two hypotheses can be put forward to account for the complex cluster chemistry that we observe in hCCS. First it is important to note that the active species is formed not in isolated hCCS but in the hCCS-SOD protein-protein complex. SOD1 is structurally homologous to D2 of hCCS, and its essential disulfide which is formed as part of the SOD1-CCS metal transfer activity, is structurally homologous to the C141-C227 disulfide cross link in hCCS. Therefore, it is possible that a polynuclear cluster similar to that formed in the hCCS homodimer or homotetramer could form in the SOD1-hCCS heterodimer/tetramer. This is illustrated in Figure 8, using the available crystal structures for the yeast heterodimer, and the human domain 2. Fig. 8(a) shows the crystal structure of the hCCS dimeric domain 2 with the cluster of Cys residues C141, C144 and C227 shown in yellow. The arrow shows where the loop formed by domain 3 is expected to be located if it follows the same orientation as in the yeast protein. The individual monomers are shown in grey/blue and gold respectively. Fig. 8 (b) shows the ySOD1-CCS heterodimer structure plotted in the same orientation as in (a) showing the interaction of the SOD and CCS D2 protomers, and CCS D3 interacting with the SOD Cys residues C57 and C146. While not identical, the protein fold is similar in human and yeast CCS D2 and SOD. If the disordered D3 of the human CCS followed the same fold seen in the heterodimer, this would place the CXC motif in close proximity to the D2 Cys ligands. Figure 8(c) shows an orientation of the 'canonical' dimer of heterodimers showing the clustering of six cysteine S atoms in the center which could conceivably reorient into a Cu_4S_6 (or similar) cluster as shown in Fig 8(d). Thus, a polynuclear Cu(I) cluster involving the Cys residues of both the CCS CXC motif and SOD C57 and/or C146 thiols is a possible intermediate during CCS-SOD interaction, and reaction of this intermediate with O_2 (21,22) would then lead to SOD disulfide formation, and transfer of copper into the SOD active site.

A second hypothesis supposes that the two clusters in hCCS could have different functions. Using Figure 8(c) as a template, removal of the SOD polypeptides (shown in gold) would generate a CCS species which could bind Cu(I) at the two CXC motifs to form a dimer, cross linked via a Cu_2S_4 dinuclear cluster. Alternatively, replacing the two SOD polypeptides with D2 of two additional CCS molecules would in the case of hCCS give rise to an entity that could form a polynuclear cluster, using D3 CXC and D2 Cys residues. Gitlin has recently shown that hCCS is degraded at high cellular copper in a process which is dependent on the presence of the D3 CXC motif (45). It is interesting to speculate that the species targeted for degradation might be a Cu_4S_6-linked tetramer which would be favored over the Cu_2S_4-linked dimer at high copper. In this scenario, the Cu_2S_4-linked dimer would act as the active species for SOD maturation by offering an open D2 interface for SOD association, as previously suggested (18). At first glance, this suggestion appears at odds with Gitlin and coworker's observation that the Y134E/G135E variant which is known to have a disrupted D2-D2 dimer interface (6), exhibits more rapid turnover than the WT protein, suggesting that the D2-D2 dimer interface must be open for recognition by the proteosomal machinery. However it is possible that energetics of formation of the polynuclear cluster compensates for dimer interface destabilization, allowing tetramer formation even in the presence of the Y134E/G135E mutation. Alternatively, the polynuclear cluster in homotetrameric hCCS may have no

function, and may never form under physiological conditions. Rather, the Cu_2S_4 dimer with an open D2 interface (18) may be the reactive form for both SOD activation and proteosomal degradation. Further studies are underway to evaluate the functional significance of the complex hCCS Cu(I) cluster chemistry.

Supplementary Material

Refer to Web version on PubMed Central for supplementary material.

Acknowledgements

References

1. Culotta VC, Klomp LWJ, Strain J, Casareno RLB, Krems B, Gitlin J. The copper chaperone for superoxide dismutase. J. Biol. Chem 1997;272:23469–23472. [PubMed: 9295278]

2. Culotta VC, Yang M, O'Halloran T,V. Activation of superoxide dismutases: Putting the metal to the pedal. Biochim. Biophys. Acta 2006;1763:747–758. [PubMed: 16828895]

3. Huffman DL, O'Halloran TV. Function, structure, and mechanism of intracellular copper trafficking proteins. Annu Rev Biochem 2001;70:677–701. [PubMed: 11395420]

4. Rosenzweig AC. Copper delivery by metallochaperone proteins. Acc Chem Res 2001;34:119–28. [PubMed: 11263870]

5. Furukawa Y, O'Halloran TV. Posttranslational modifications in Cu,Znsuperoxide dismutase and mutations associated with amyotrophic lateral sclerosis. Antioxid Redox Signal 2006;8:847–67. [PubMed: 16771675]

6. Schmidt PJ, Kunst C, Culotta VC. Copper activation of superoxide dismutase 1 (SOD1) *in vivo*. Role for protein-protein interactions with the copper chaperone for SOD1. J. Biol. Chem 2000;275:33771–33776. [PubMed: 10944535]

7. Schmidt PJ, Rae TD, Pufahl RA, Hamma T, Strain J, O'Halloran TV, Culotta VC. Multiple protein domains contribute to the action of the copper chaperone for superoxide dismutase. J. Biol. Chem 1999;274:23719–23725. [PubMed: 10446130]

8. Hall LT, Sanchez RL, Holloway SP, Zhu H, Stine JE, Lyons TJ, Demeler B, Schirf V, Hansen JC, Nersissian AM, Valentine JS, Hart PJ. X-ray crystallographic and ultracentrifugation analyses of truncated and full-length copper chaperones for SOD (LYS7). A dimer-dimer model of LYS7-SOD association and copper delivery. Biochemistry 2000;39:3611–3623. [PubMed: 10736160]

9. Lamb AL, Torres AS, O'Halloran TV, Rosenzweig AC. Heterodimeric structure of superoxide dismutase in complex with its metallochaperone. Nat. Struct. Biol 2001;8:751–755. [PubMed: 11524675]

10. Lamb AL, Wernimont AK, Pufahl RA, Culotta VC, O'Halloran TV, Rosenzweig AC. Crystal structure of the copper chaperone for superoxide dismutase. Nat. Struct. Biol 1999;6:724–729. [PubMed: 10426947]

11. Lamb AL, Wernimont AK, Pufahl RA, O'Halloran TV, Rosenzweig AC. Crystal structure of the second domain of the human copper chaperone for superoxide dismutase. Biochemistry 2000;39:1589–1595. [PubMed: 10677207]

12. Arnesano F, Banci L, Bertini I, Huffman D, O'Halloran TV. Solution structure of the Cu(I) and apo forms of the yeast metallochaperone Atx1. Biochemistry 2001;40:1528–1539. [PubMed: 11327811]

13. Portnoy ME, Rosenzweig AC, Rae T, Huffman DL, O'Halloran TV, Culotta VC. Structure-function analyses of the ATX1 metallochaperone. J. Biol. Chem 1999;274:15041–15045. [PubMed: 10329707]

14. Rosenzweig AC, Huffman DL, Hou MY, Wernimont AK, Pufahl RA, O'Halloran TV. Crystal Structure of the Atx1 metallochaperone protein at 1.02 Å resolution. Structure 1999;7:605–617. [PubMed: 10404590]

15. Wernimont AK, Huffman DL, Lamb AL, O'Halloran TV, Rosenzweig AC. Structural basis for copper transfer by the metallochaperone for Menkes/Wilson disease proteins. Nat. Struct. Biol 2000;7:766–771. [PubMed: 10966647]

16. Ralle M, Lutsenko S, Blackburn NJ. X-ray absorption spectroscopy of the copper chaperone HAH1 reveals a linear 2-coordinate Cu(I) center capable of adduct formation with exogenous thiols and phosphines. J. Biol. Chem 2003;278:23163–23170. [PubMed: 12686548]

17. Stasser JP, Eisses JF, Barry AN, Kaplan JH, Blackburn NJ. Cysteine-to-serine mutants of the human copper chaperone for superoxide dismutase reveal a copper cluster at a domain III dimer interface. Biochemistry 2005;44:3143–52. [PubMed: 15736924]

18. Stasser J, Siluvai GS, Barry AN, Blackburn NJ. A multinuclear copper (I) cluster forms the dimerization interface in copper-loaded human copper chaperone for superoxide dismutase. Biochemistry 2007;46:11845–11856. [PubMed: 17902702]

19. Torres AS, Petri V, Rae TD, O'Halloran TV. Copper stabilizes a heterodimer of the yCCS metallochaperone and its target superoxide dismutase. J. Biol. Chem 2001;276:38410–38416. [PubMed: 11473116]

20. Lamb AL, Torres AS, O'Halloran TV, Rosenzweig AC. Heterodimer formation between superoxide dismutase and its copper chaperone. Biochemistry 2000;39:14720–14727. [PubMed: 11101286]

21. Furukawa Y, Torres AS, O'Halloran TV. Oxygen-induced maturation of SOD1: a key role for disulfide formation by the copper chaperone CCS. EMBO J 2004;23:2872–2881. [PubMed: 15215895]

22. Brown NM, Torres AS, Doan PE, O'Halloran TV. Oxygen and the copper chaperone CCS regulate posttranslational activation of Cu,Zn superoxide dismutase. Proc. Natl. Acad. Sci. U. S. A 2004;101:5518–5523. [PubMed: 15064408]

23. Banci L, Bertini I, Cantini F, D'Amelio N, Gaggelli E. Human SOD1 before harboring the catalytic metal: solution structure of copper-depleted, disulfide-reduced form. J Biol Chem 2006;281:2333–7. [PubMed: 16291742]

24. Rae PJ, Schmidt PJ, Pufahl RA, Culotta VC, O'Halloran TV. Undetectable intracellular free copper: the requirement of a copper chaperone for superoxide dismutase. Science 1999;284:805–808. [PubMed: 10221913]

25. Rae TD, Torres AS, Pufahl RA, O'Halloran TV. Mechanism of Cu, Zn-superoxide dismutase activation by the human metallochaperone hCCS. J. Biol. Chem 2001;276:5166–5176. [PubMed: 11018045]

26. Eisses JF, Stasser JP, Ralle M, Kaplan J, Blackburn NJ. Domains I and III of the human copper chaperone for superoxide dismutase interact via a cysteine-bridged dicopper cluster. Biochemistry 2000;39:7337–7342. [PubMed: 10858280]

27. Barry AN, Blackburn NJ. A Selenocysteine Variant of the Human Copper Chaperone for Superoxide Dismutase. A Se-XAS Probe of Cluster Composition at the Domain 3-Domain 3 Dimer Interface. Biochemistry 2008;49:4916–4928. [PubMed: 18393442]

28. Gieselman MD, Xie L, van der Donk WA. Synthesis of a selenocysteine-containing peptide by native chemical ligation. Org. Lett 2001;3:1331–1334. [PubMed: 11348227]

29. Harris KM, Flemer S Jr. Hondal RJ. Studies on deprotection of cysteine and selenocysteine side-chain protecting groups. J. Pept. Sci 2007;13:81–93. [PubMed: 17031870]

30. George, GN. EXAFSPAK. Menlo Park; CA: 1990.

31. Binsted, N.; Gurman, SJ.; Campbell, JW. EXCURVE *9.2*. Warrington; England: 1998.

32. Gurman SJ, Binsted N, Ross I. A rapid, exact, curved-wave theory for EXAFS calculations. J. Phys. C 1984;17:143–151.

33. Gurman SJ, Binsted N, Ross I. A rapid, exact, curved-wave theory for EXAFS calculations. II. The multiple-scattering contributions. J. Phys. C 1986;19:1845–1861.

34. Binsted N, Hasnain SS. State of the art analysis of whole X-ray absorption spectra. J. Synchrotron Rad 1996;3:185–196.

35. Blackburn NJ, Rhames FC, Ralle M, Jaron S. Major changes in copper coordination accompany reduction of peptidylglycine monooxygenase. J. Biol. Inorg. Chem 2000;5:341–353. [PubMed: 10907745]

36. Dance IG, Calabrese JC. The crystal and molecular structure of the hexa-(μ_2-benzenethiolato) tetracuprate(I) dianion. Inorg. Chim. Acta 1976;19:L41–L42.

37. Pickering IJ, George GN, Dameron CT, Kurz B, Winge DR, Dance IG. X-ray absorption spectroscopy of cuprous-thiolate clusters in proteins and model systems. J. Am. Chem. Soc 1993;115:9498–9505.

38. Brown KR, Keller GL, Pickering IJ, Harris HH, George GN, Winge DR. Structures of the cuprous-thiolate clusters of the Mac1 and Ace1 transcriptional activators. Biochemistry 2002;41:6469–76. [PubMed: 12009910]

39. Lobana TS, Rimple Castineiras, A. Turner P. Copper-selenium interactions: influence of alkane spacer and halide anion in the synthesis of unusual polynuclear copper(I) complexes with bis (diphenylselenophosphinyl)alkanes. Inorg. Chem 2003;42:4731–4737. [PubMed: 12870965]

40. Nitschke C, Fenske D, Corrigan JF. Ferrocenyldiselenolate-stabilized copper-selenium clusters. Inorg. Chem 2006;45:9394–9401. [PubMed: 17083239]

41. Christuk CC, Ansari MA, Ibers JA. Interactions of coinage-group cations with the tetraselenotungstate anion: multinuclear NMR spectroscopic results and crystal structures of $(\mu\text{-}WSe_4)[PMe_2Ph]_2Cu]_2$, $(\mu\text{-}WSe_4)[PMePh_2)Au]_2$ and $(\mu_3\text{-}Cl)(\mu_3\text{-}WSe_4)[(PPh_3)Cu]_3$. Inorg. Chem 1992;31:4365–4369.

42. Salm RJ, Ibers JA. Synthesis, structure, and spectroscopy of $[PPh_4]_2[(NC)Cu(\mu\text{-}Se)_2M(\mu\text{-}Se)_2Cu(CN)]\cdot CH_3CN$ and $[PPh_4]_2[(NC)Cu(\mu\text{-}Se)_2MSe_2$ (M=Mo, W). Inorg. Chem 1994;33:4216–4220.

43. Deveson A, Dehnen S, Fenske D. Synthesis and structures of four new copper(I)-selenium clusters: size dependence of the cluster on the reaction conditions. J. Chem. Soc. Dalton Trans 1996;1997:4491–4497.

44. Liu CW, Hung CM, Santra BK, Wang JC, Kao HM, Lin Z. Ligand substitution in cubic clusters: surprising isolation of the cocrystallization products of $Cu_8(\mu_8\text{-}Se)[S_2P(OEt)_2]_6$ and $Cu_6[S_2P(OEt)_2]_6$. Inorg. Chem 2003;42:8551–6. [PubMed: 14658912]

45. Caruano-Yzermans AL, Bartnikas TB, Gitlin JD. Mechanisms of the copper-dependent turnover of the copper chaperone for superoxide dismutase. J. Biol. Chem 2006;281:13581–13587. [PubMed: 16531609]
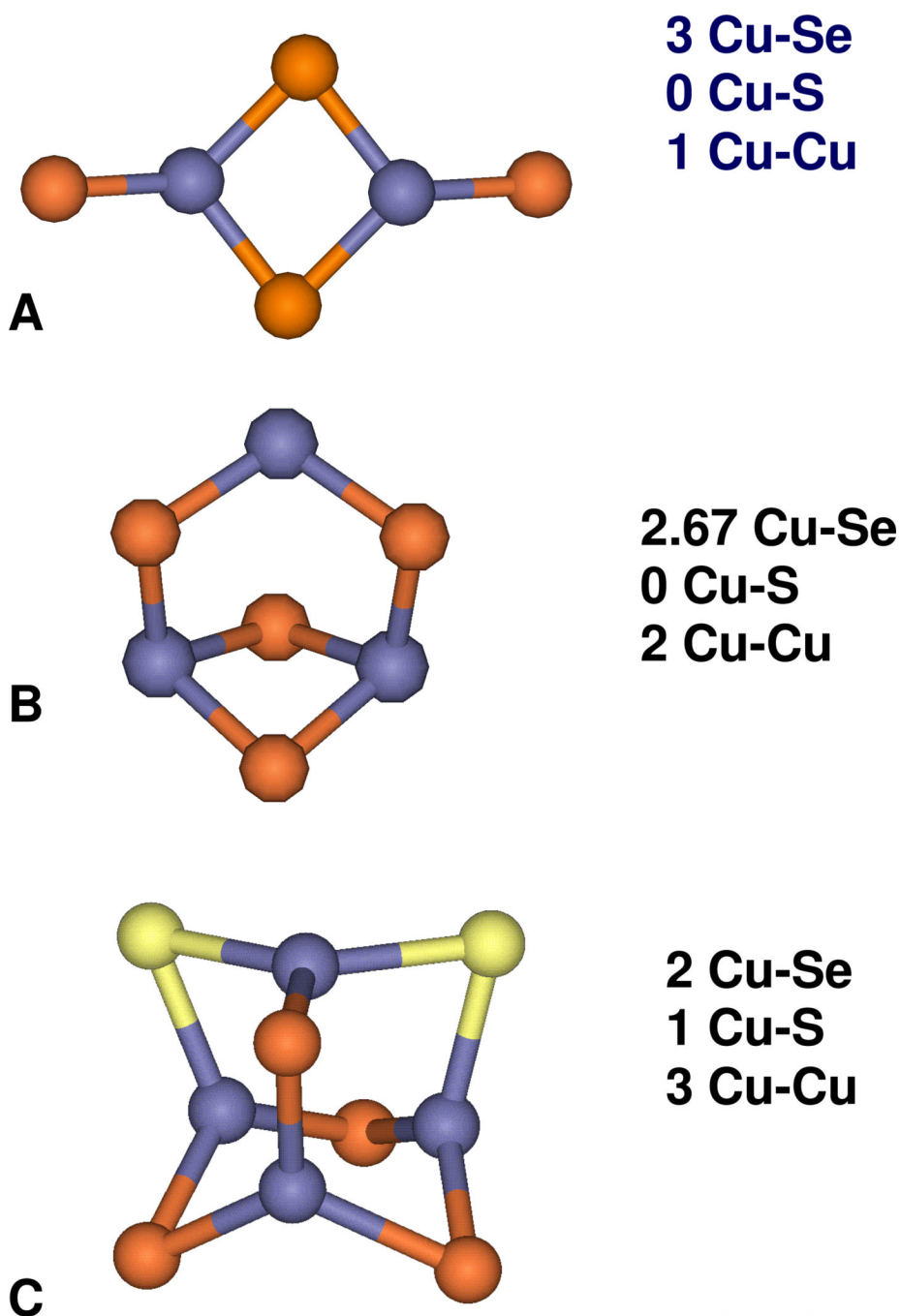
3 Cu-Se
0 Cu-S
1 Cu-Cu

2.67 Cu-Se
0 Cu-S
2 Cu-Cu

2 Cu-Se
1 Cu-S
3 Cu-Cu

Figure 1.
Possible structures for the hCCS multinuclear cluster. A, Cu_2S_4 bis-cysteine bridged dinuclear species, with one terminal and two bridging Cys residues per copper, and a single Cu-Cu interaction; B, Cu_3S_4 with only bridging Cys residues and two Cu-Cu interactions; C, Cu_4S_6 "adamantane" type cluster with only bridging Cys and three Cu-Cu interactions. The expected shell occupancy for the 243-UAUA derivative is given alongside each structure.
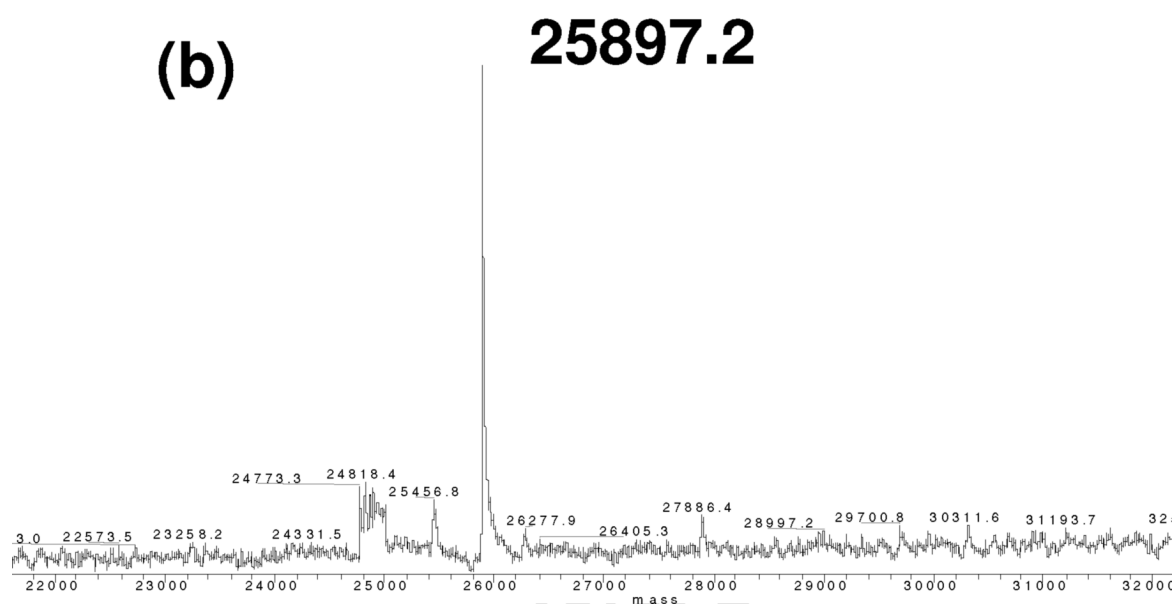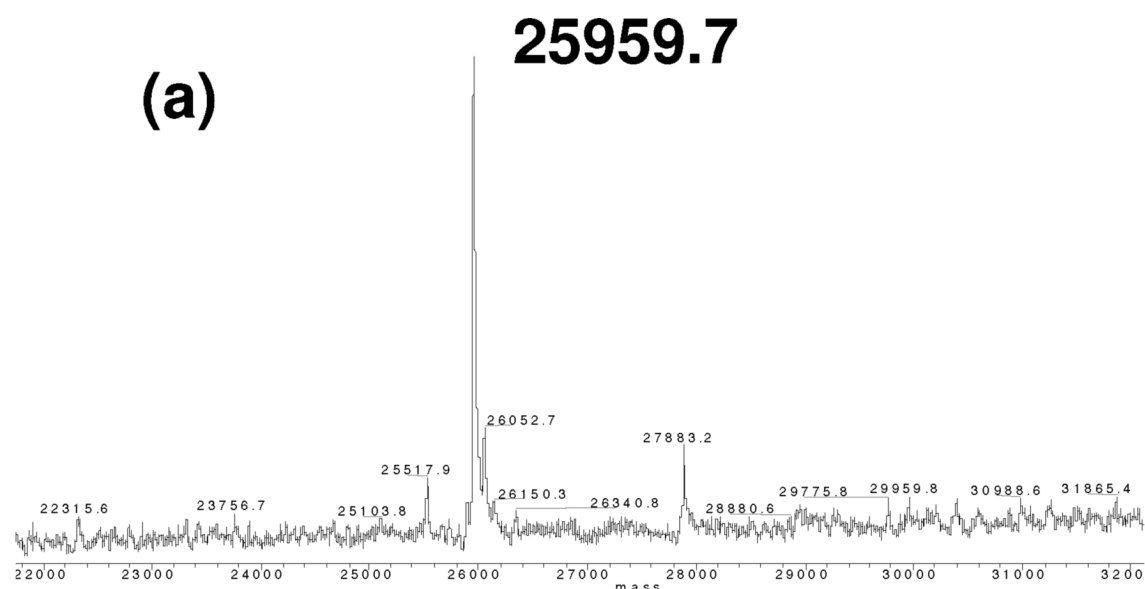
Figure 2.
ESI mass spectrometry of (a) 243-UAUA in a WT background and (b) 243-UAUA in a C22AC25A background.
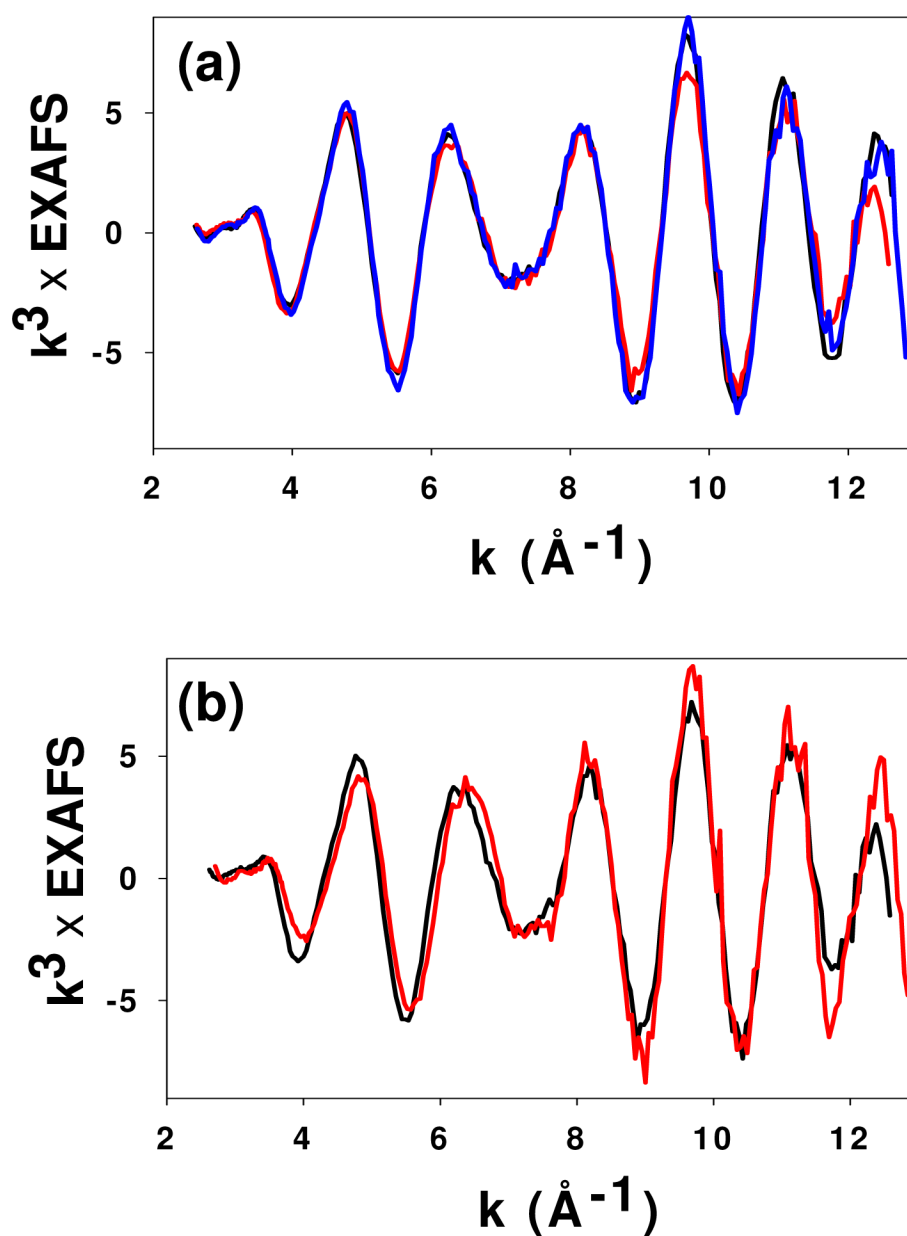
Figure 3.
Comparison of experimental EXAFS for Sec positional variants of hCCS in the C22AC25A background. (a) 243-UACA and 243-CAUA and (b) 243-UACA and 243-UAUA.

Figure 4.
Fourier transforms and EXAFS (top inset) for the 243-UACA variant of hCCS in the
C22AC25A background. (a) Cu K-EXAFS data, (b) Se K-EXAFS data. Black traces represent
experimental data, red traces represent simulated data. Parameters used in the fits are listed in
Table 2. Absorption edges are shown in the bottom insets.
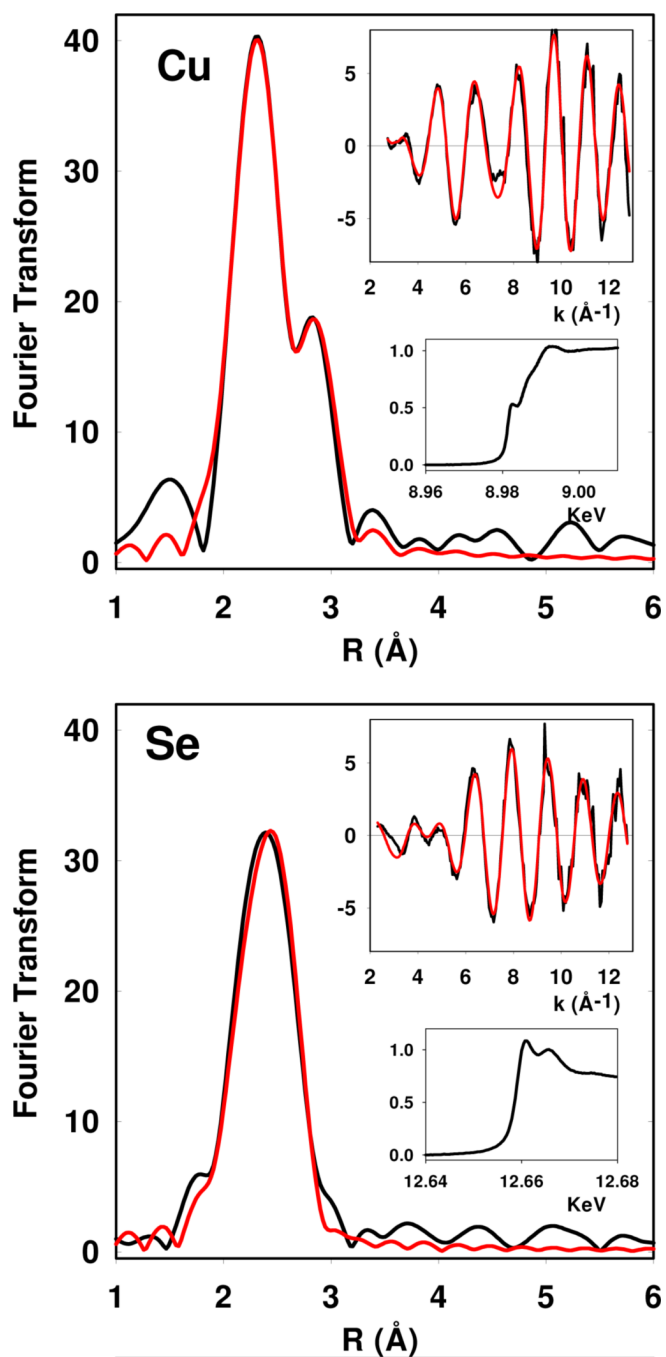
Figure 5.
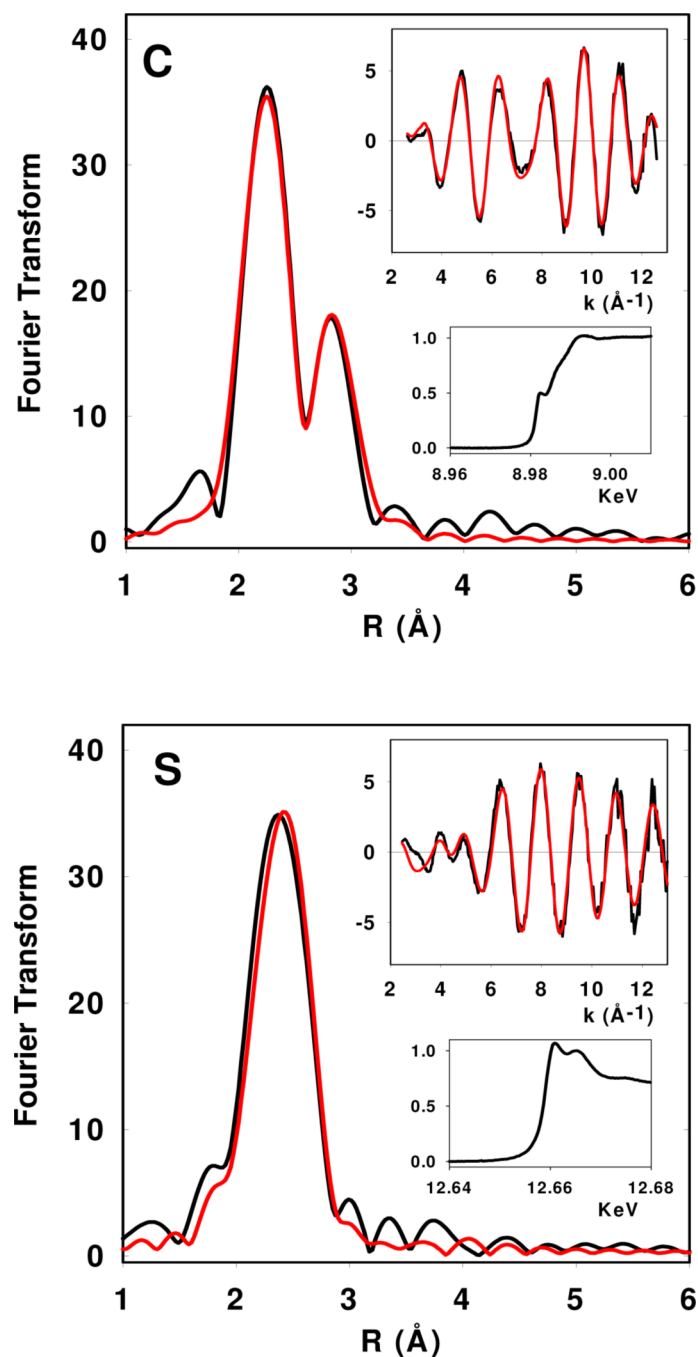Fourier transforms and EXAFS (top inset) for the 243-UAUA variant of hCCS in the C22AC25A background. (a) Cu K-EXAFS data, (b) Se K-EXAFS data. Black traces represent experimental data, red traces represent simulated data. Parameters used in the fits are listed in Table 2. Absorption edges are shown in the bottom insets.
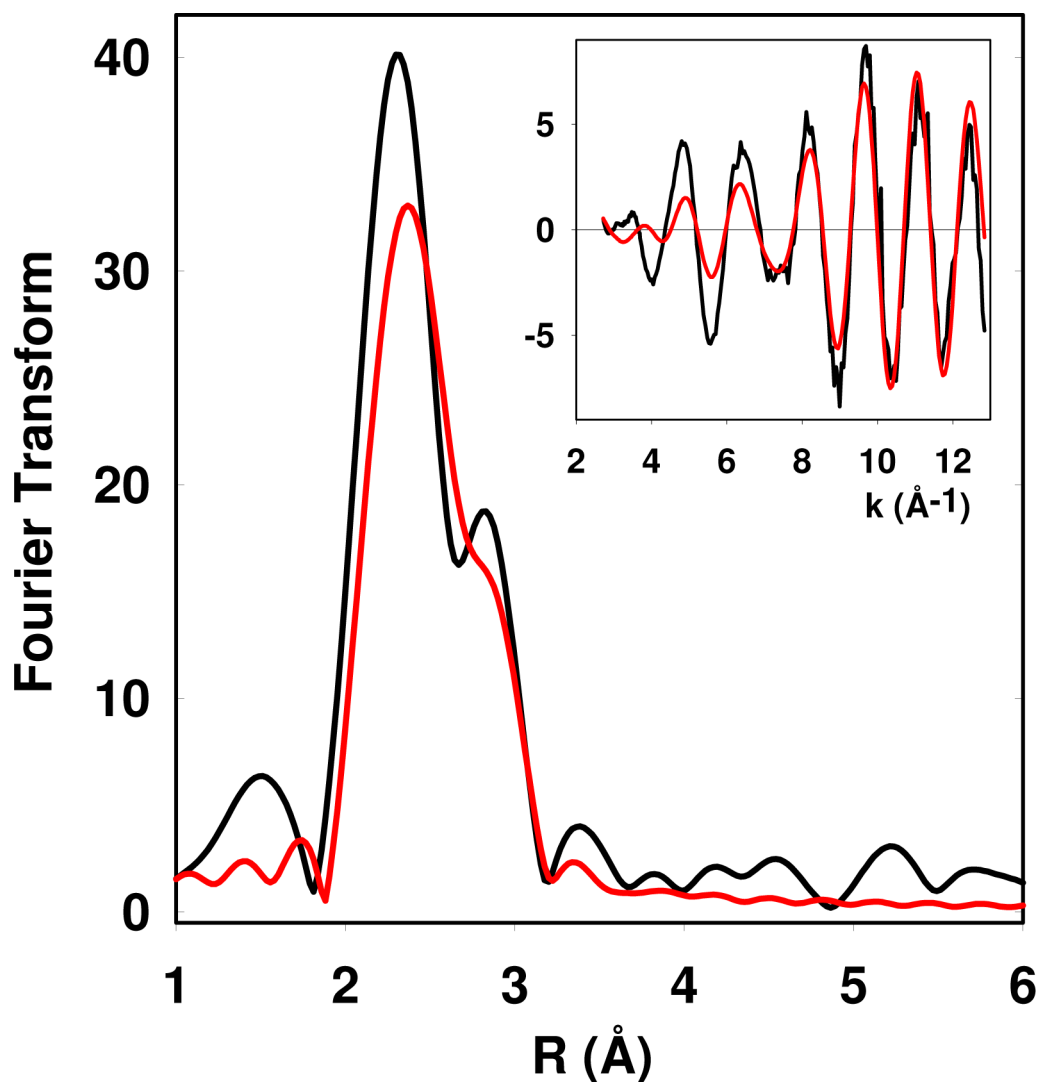
Figure 6.
Cu- K EXAFS and Fourier transform of the 243-UAUA variant of hCCS in the C22AC25A background simulated with no S backscattering. Black traces represent experimental data, red traces represent simulated data. Parameters used in the fits are listed in Table 2 (243-UAUA no S fit).
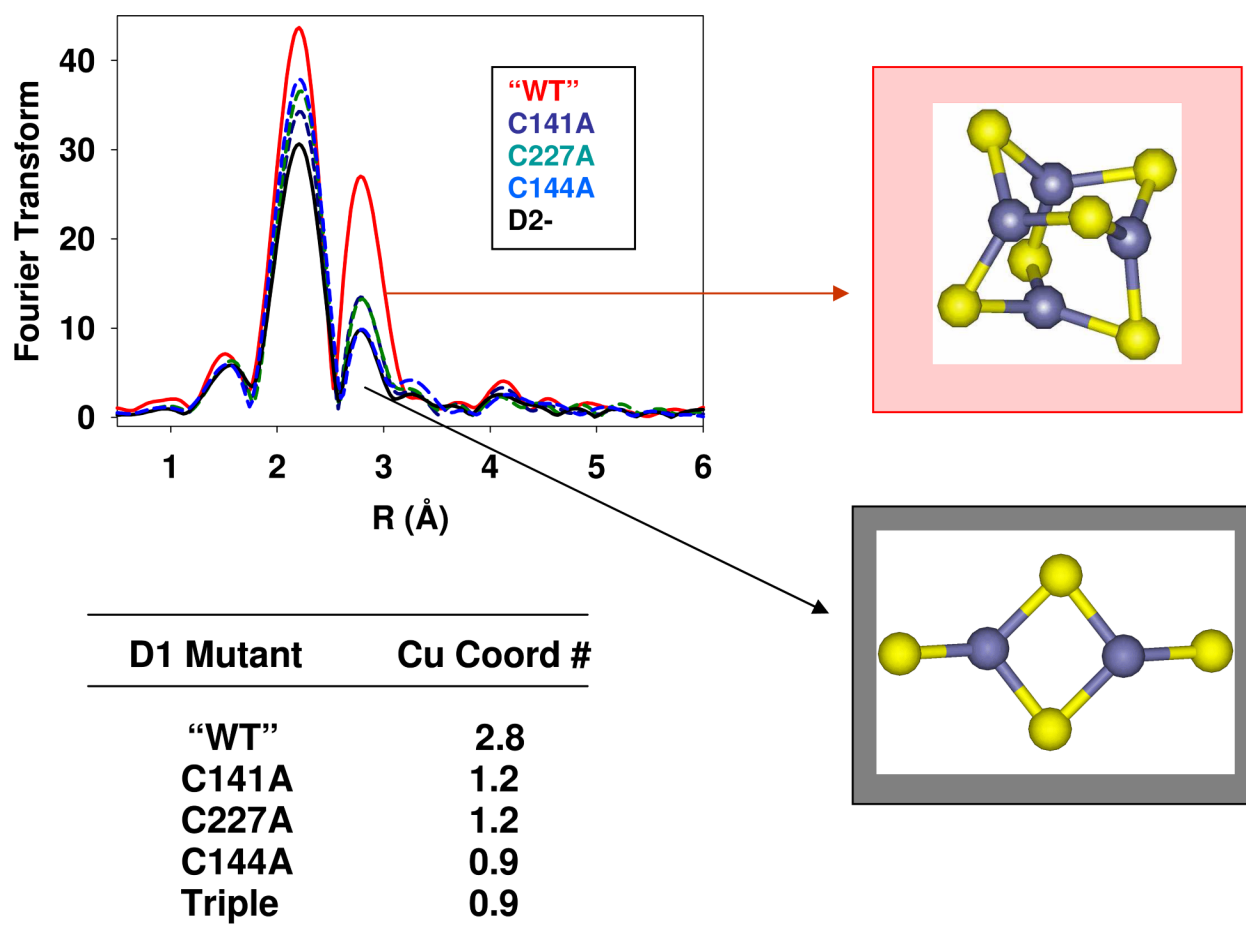
Figure 7.
Comparison of experimental Fourier transforms for Domain 2 Cys to Ala single variants and the D2 Cys to Ala triple mutant (C22AC25A background). WT, red trace; C141A, dark blue trace; C227A green trace; C144A, light blue trace; C141A/C144A/C227A triple mutant, black trace. Simulations (Table 3) were used to generate the Cu-Cu shell occupancies for each variant.
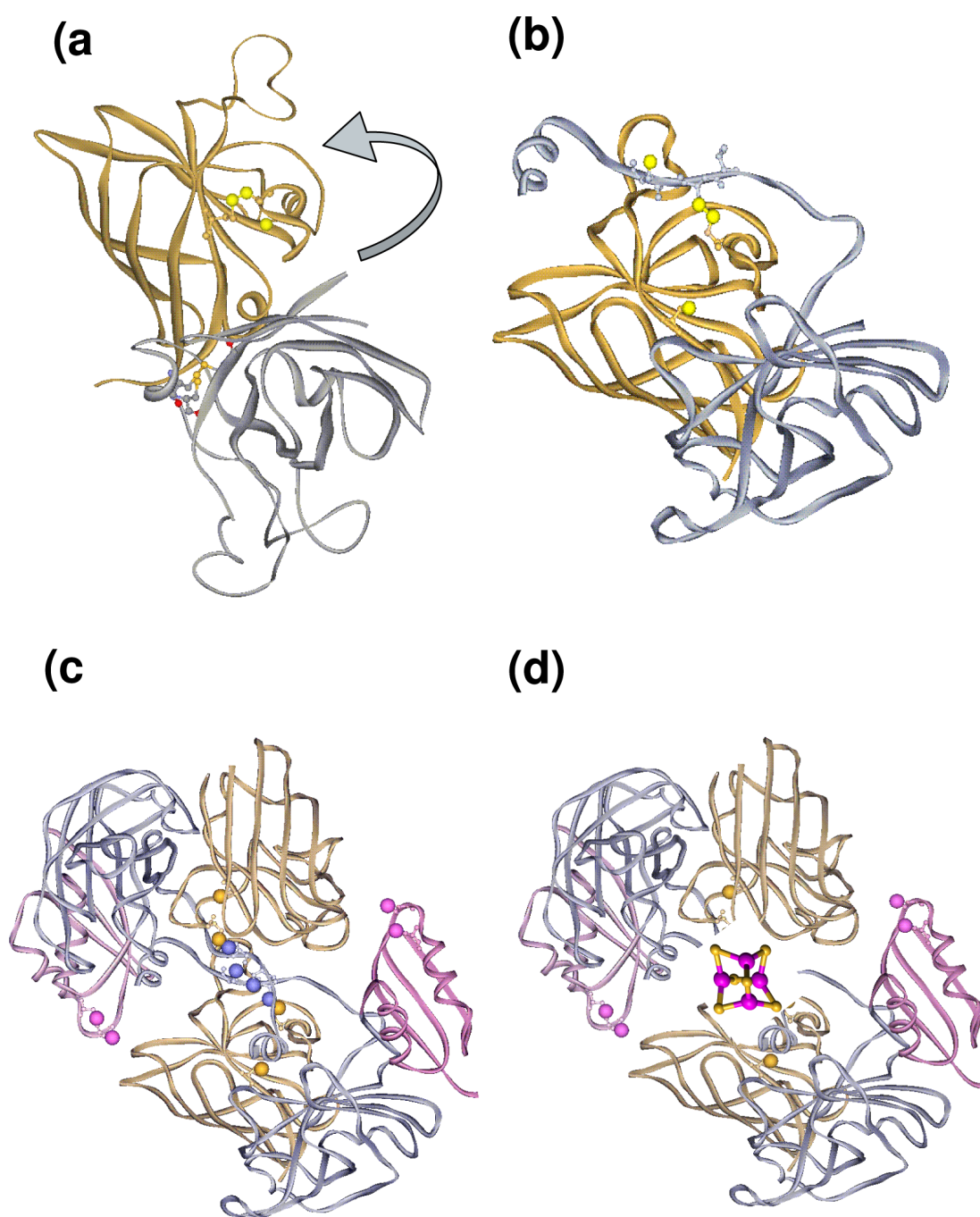
Figure 8.
(a) Crystal structure of the hCCS dimeric domain 2 with the cluster of Cys residues C141, C144 and C227 shown in yellow. The arrow shows where the loop formed by domain 3 is expected to be located if it follows the same orientation as in the yeast protein. The individual monomers are shown in grey/blue and gold respectively. (b) The ySOD1-CCS heterodimer structure plotted in the same orientation as in (a) showing the interaction of the SOD and CCS D2 protomers, and CCS D3 interacting with the SOD Cys residues C57 and C146. (c) Tetrameric form of the ySOD1-CCS heterostructure showing the location of all of the Cys residues from SOD (gold) and CCS (grey/blue). (d) Cartoon representation of the multinuclear cluster utilizing Cys residues from both SOD (or hCCS) and D3 (CCS) polypeptides. In (b) –

(d), SOD is color coded gold, while CCS is blue/grey (D2) or pink (D1). Coordinates for the hCCS D2 and ySOD-CCS heterodimer structures were taken from PDB files 1DO5 and 1JK9 respectively.

Table 1

Calculated and observed masses for Se positional variants of hCCS determined by electrospray mass spectrometry.

Protein	*m/z* Calc	*m/z* Calc. Met1 cleaved	*m/z* Observed	Activity (percent of WT hCCS)
243-CACA	26001	25870	25863	55 ± 8
243-CAUA	26048	25917	25912	98 ± 13
243-UACA	26048	25917	25907	93 ± 11
243-UAUA	26095	25964	25960	89 ± 13
C22AC25A 243-CACA	25937	25806	25800	75 ± 5
C22AC25A 243-CAUA	25984	25853	25851	70 ± 8
C22AC25A 243-UACA	25984	25853	25844	65 ± 6
C22AC25A 243-UAUA	26031	25800	25897	84 ± 7

Table 2

Fits obtained to the Cu and Se K-EXAFS of hCCS Sec positional variants by curve-fitting using the program EXCURVE 9.2.

sample	F^a	Cu-S			Cu-Se			Cu-Cu			$-E_0$
		N_o^b	$R (\text{Å})^c$	DW (Å^2)	N_o^b	$R (\text{Å})^c$	DW (Å^2)	N_o^b	$R (\text{Å})^c$	DW (Å^2)	
Cu EXAFS											
243-CACA	0.310	3.0	2.26	0.009				2.0	2.72	0.012	5.20
243-CAUA	0.129	1.6	2.22	0.004	1.0	2.40	0.007	2.8	2.70	0.012	2.07
243-UACA	0.255	1.8	2.22	0.005	1.0	2.42	0.007	2.3	2.70	0.012	1.91
243-UAUA	0.381	1.1	2.18	0.003	1.9	2.40	0.007	2.6	2.70	0.012	0.40
243-UAUA (no sulfur)	1.454				1.9	2.38	0.007	2.1	2.69	0.012	0.04
Se EXAFS		Se-C			Se-Cu						
243-CAUA	0.285	1.0	1.98	0.010	2.0	2.37	0.007				3.08
243-UACA	0.551	1.0	1.99	0.010	1.9	2.38	0.007				2.92
243-UAUA	0.474	1.0	2.02	0.005	1.9	2.39	0.007				5.37

[a] F is a least-squares fitting parameter defined as $F^2 = \frac{1}{N}\sum_{i=1}^{N} k^6 \left(Data - Model \right)^2$

[b] The precision in the estimated coordination numbers is generally considered to be ±25%

[c] In any one fit, the statistical error in bond-lengths is ±0.005 Å. However, when errors due to imperfect background subtraction, phase-shift calculations, and noise in the data are compounded, the actual error is probably closer to ±0.02 Å.

Table 3

Fits obtained to the Cu and Se K-EXAFS of CCS-C22AC25A domain 2 Cys to Ala mutants using the program EXCURVE 9.2.

Cu EXAFS

sample	F^a	Cu-S No^b	Cu-S $R(\text{Å})^c$	Cu-S $DW(\text{Å}^2)$	Cu-Se No^b	Cu-Se $R(\text{Å})^c$	Cu-Se $DW(\text{Å}^2)$	Cu-Cu No^b	Cu-Cu $R(\text{Å})^c$	Cu-Cu $DW(\text{Å}^2)$	$-E_0$
C141A	0.365	3	2.25	0.012				1.2	2.72	0.012	4.83
C144A	0.431	3	2.25	0.011				0.9	2.72	0.012	5.20
C227A	0.392	3	2.25	0.011				1.2	2.71	0.012	4.33
Triple	0.413	3	2.24	0.013				0.9	2.71	0.012	4.34
Triple UAUA	0.535	0.5	2.17	0.005	2.0	2.38	0.006^d	2.0	2.71	0.008^d	0.70

Se EXAFS

sample	F^a	Se-C No^b	Se-C $R(\text{Å})^c$	Se-C $DW(\text{Å}^2)$	Se-Cu No^b	Se-Cu $R(\text{Å})^c$	Se-Cu $DW(\text{Å}^2)$
Triple UAUA		1	1.99	0.007	2	2.39	0.006^d

[a] F is a least-squares fitting parameter defined as $F^2 = \dfrac{1}{N}\sum_{i=1}^{N} k^6 \left(Data - Model \right)^2$

[b] The precision in the estimated coordination numbers is generally considered to be ± 25%

[c] In any one fit, the statistical error in bond-lengths is ±0.005 Å. However, when errors due to imperfect background subtraction, phase-shift calculations, and noise in the data are compounded, the actual error is probably closer to ±0.02 Å.

[d] The Cu cluster in the triple UAUA fit appeared to have different structural parameters from other variants, particularly the Cu-Cu and Se-Cu DW factors. This aberrant chemistry is discussed further in the text.